Alqalam Journal of Medical and Applied Sciences. 2026;9(11):3532-3544
https://doi.org/10.54361/ajmas.261101

Original article

A Reduced-Order Reaction-Diffusion Model of Localised Nanoparticle-Mediated Payload Delivery and Tumor Response in Osteosarcoma

Khadija Hassan

Department of Mathematics, Faculty of Science, Sabratha University
Email. *Khadija.abdelatif@sabu.edu.ly*

Abstract
Osteosarcoma treatment is influenced not only by tumor proliferation but also by the spatial delivery of therapeutic agents and the extent to which delivered material becomes therapeutically active inside tumor cells. We present a deliberately reduced one-dimensional reaction-diffusion model that separates extracellular nanoparticle transport from an effective intracellular active-payload exposure state. The model couples normalised tumor density, extracellular nanoparticle concentration, and intracellular exposure through logistic tumor growth, Fickian diffusion of tumor cells and nanoparticles, first-order nanoparticle clearance, cell-associated uptake, intracellular payload loss, and payload-dependent tumor-cell death. A localised Gaussian source is normalised by its spatial integral, making total input independent of mesh resolution. Symmetric outward Robin leakage is imposed at the domain boundaries. The method-of-lines system is solved with a stiff BDF solver, and numerical reliability is assessed by mesh refinement, tolerance checks, nonnegativity monitoring, and a matched untreated control. At the illustrative baseline, centre tumor density falls from 0.8000 initially to 0.718891 at day 5, whereas the untreated control reaches 0.9359. The corresponding endpoint centre reduction is 23.18%; the spatially averaged burden is 12.70% lower, and the five-day integrated burden is 5.56% lower. Refinement from 161 to 321 nodes changes the centre value by 0.023%, with an observed second-order refinement rate. A structural comparison with the predecessor two-state formulation shows why the interpretation of the uptake coefficient β depends on model structure: β has a negative normalised sensitivity (-0.177) in the three-state model but a positive sensitivity (+0.128) when uptake is treated only as extracellular nanoparticle removal. The model is therefore positioned as a transparent mechanistic and numerical framework for hypothesis generation, not as a clinically validated predictive tool.
Keywords. Osteosarcoma; Reaction-Diffusion; Nanoparticle Delivery; Intracellular Exposure.

Introduction

Osteosarcoma is an aggressive primary bone malignancy for which local disease control is influenced by tumor biology, treatment penetration, and the heterogeneous transport properties of the tumor microenvironment [1,2]. Nanoparticle-based delivery systems have attracted interest because they can alter drug localisation, release, and exposure, but successful delivery to solid tumors remains constrained by transport barriers and by the sequence linking tissue penetration to cellular uptake and intracellular drug action [3,4,8]. These considerations are particularly relevant to osteosarcoma, where nanomedicine strategies increasingly emphasise targeted delivery and controlled release [2]. Mathematical models are useful in this setting because they make assumptions about transport, uptake, and treatment response explicit and allow their consequences to be explored systematically [3,4]. However, model complexity does not automatically improve predictive value. Mechanism-based oncology models require quantitative measurements for calibration, and predictions should be evaluated against independent data whenever possible [5]. The present study originated from a two-state reaction-diffusion formulation in which tumor density and extracellular nanoparticle concentration were coupled directly through an uptake/removal term and a treatment-killing term. A rigorous audit showed that this structure made the biological meaning of the uptake coefficient ambiguous [3,4,8]: increasing uptake could remove nanoparticles from the extracellular compartment without increasing a distinct intracellular therapeutic exposure. The revised model therefore introduces a third state, w, interpreted as an effective intracellular active-payload exposure field. This is intentionally a reduced-order representation; it does not claim to resolve receptor binding, endocytosis, intracellular trafficking, release chemistry, or detailed pharmacokinetics.

The central question is consequently not whether a particular nanoparticle formulation is clinically effective, but whether explicit separation of extracellular transport from intracellular active exposure changes the interpretation of treatment response and parameter sensitivity. The study contributes (i) a dimensionally consistent three-state reaction-diffusion model, (ii) a grid-independent localised source and boundary-consistent Robin discretisation, (iii) a boundary-aware stability benchmark, (iv) reproducible mesh and tolerance analysis, and (v) a direct structural comparison with the predecessor two-state formulation.

Mathematical Model Methods

Let $u(x,t)$ be normalised tumor-cell density, $v(x,t)$ normalised extracellular nanoparticle concentration, and $w(x,t)$ normalised effective intracellular active-payload exposure. The one-dimensional Cartesian surrogate domain is $0 \le x \le L$ and t is measured in days. The normalisation sets $K = 1$ as the reference tumor carrying capacity and $v = 1$ as the reference extracellular concentration. The assumptions are intentionally parsimonious: homogeneous one-dimensional transport; logistic tumor proliferation; Fickian diffusion of tumor cells and extracellular nanoparticles; first-order extracellular clearance; uptake proportional to uv; conversion of uptake into effective intracellular exposure; first-order intracellular

Copyright *Author (s) 2026. Distributed under Creative Commons CC BY 4.0*
Received*: 26-08-2026 -* ***Accepted****: 24-10-2026 -* ***Published****: 01-11-2026*

https://doi.org/10.54361/ajmas.261101

payload loss; and tumor-cell loss proportional to uw. The source is localised in space but continuous over the five-day numerical window. Because w is an effective exposure state rather than a conserved intracellular mass, no separate diffusion coefficient is assigned to w. This physically reflects the assumption that once therapeutic payloads cross the cell membrane, they become bound or entrapped within the local cellular architecture, rendering their free lateral interstitial diffusion negligible compared to the unhindered extracellular transport of nanoparticles (v). The model should therefore not be read as a literal intracellular mass-balance model.

Governing Equations and Boundary Conditions

$$\frac{\partial u}{\partial t} = D_u \frac{\partial^2 u}{\partial x^2} + ru\left(1 - \frac{u}{K}\right) - \delta uw \quad (1)$$

$$\frac{\partial v}{\partial t} = D_v \frac{\partial^2 v}{\partial x^2} - \lambda v - \beta uv + q(x) \quad (2)$$

$$\frac{\partial w}{\partial t} = \beta uv - k_w w \quad (3)$$

$$q(x) = \frac{Qg(x)}{\int_0^L g(\xi)d\xi}\ , \quad g(x) = \exp[-\frac{(x-\frac{L}{2})^2}{2\sigma_q^2}] \quad (4)$$

$$-D_u u_x(0,t) = \gamma_u u(0,t), \quad -D_u u_x(L,t) = \gamma_u u(L,t) \quad (5)$$

$$-D_v v_x(0,t) = \gamma_v v(0,t), \quad -D_v v_x(L,t) = \gamma_v v(L,t) \quad (6)$$

The source normalisation implies $\int q(x)dx = Q$. Because v is dimensionless and q enters the v-equation as a rate, Q has units of mm/day in this formulation. This dimensional point is important for mesh-independent reproducibility. The equations (5) and (6) define symmetric outward Robin leakage, where the negative sign on the flux matches the outward normal vectors at the domain bounds to align completely with the conservation mechanics applied in numerical implementation.

Baseline Parameter Set

All baseline values are illustrative computational parameters. They are not presented as experimentally measured or patient-specific osteosarcoma constants. See (Table 1) for baseline model parameters.

Table 1. Baseline model parameters

Symbol	Meaning	Value	Unit
L	Domain length	10	mm
D_u	Tumor-cell effective diffusion/motility	0.01	mm^2/day
D_v	Extracellular nanoparticle diffusion	0.25	mm^2/day
r	Tumor proliferation rate	0.40	day^{-1}
K	Reference carrying capacity	1.00	Dimensionless
δ	Tumor-cell loss coefficient	0.50	day^{-1}
λ	Extracellular clearance rate	0.10	day^{-1}
β	Uptake-to-intracellular-exposure rate	0.60	day^{-1}
k_w	Intracellular exposure loss rate	0.25	day^{-1}
γ_u	Tumor-cell Robin leakage	0.05	mm/day
γ_v	Nanoparticle Robin leakage	0.12	mm/day
Q	Integrated localised source strength	0.30	mm/day
σ_q	Source width	0.25	mm
$\sigma_{u,0}$	Initial tumor width	0.50	mm
T	Simulation horizon	5.0	day
N_x	Baseline grid points	161	-

Stability Benchmark

For the full Robin problem, the constant tumor-bearing state $(K, 0,0)$ is not an equilibrium when $\gamma_u > 0$ because a spatially constant positive u cannot satisfy nonzero outward leakage. The stability calculation is therefore presented as a kinetic/zero-flux benchmark rather than as a claim about therapeutic efficacy. For the zero-flux benchmark, the linearization about $E_1 = (K, 0,0)$ for spatial mode k has eigenvalues $-r - D_u k^2$, $-(\lambda + \beta K) - D_v k^2$, and $-k_w$. All are negative for positive parameters. This establishes local asymptotic stability of the benchmark equilibrium only; it does not establish tumor-tumor control under treatment. For the actual leakage problem, $E_0 = (0,0,0)$ is boundary-compatible. The tumor-tumor component near E_0 has a model growth rate $r - D_u \mu_n$, where μ_n are Robin Laplacian eigenvalues. This analysis is used only to characterise the mathematical structure of the system.

Spatial Discretisation and Time Integration

Second-order central finite differences are used in the interior. Ghost-point elimination gives the left and right boundary approximations

Copyright *Author (s) 2026. Distributed under Creative Commons CC BY 4.0*
Received*: 26-08-2026 -* ***Accepted****: 24-10-2026 -* ***Published****: 01-11-2026*

https://doi.org/10.54361/ajmas.261101

$$u_{xx}(0) \approx \frac{2[u_1 - u_0 - \left(\frac{\gamma_u \Delta x}{D_u}\right)u_0]}{\Delta x^2} \quad (7)$$

$$u_{xx}(L) \approx \frac{2[u_{N-2} - u_{N-1} - \left(\frac{\gamma_u \Delta x}{D_u}\right)u_{N-1}]}{\Delta x^2} \quad (8)$$

Analogous expressions are used for v. The semi-discrete system is integrated with MATLAB ode15s, a stiff BDF-type solver, using RelTol = 10^{-7} and AbsTol =10^{-9} in the reference implementation. The baseline grid has 161 nodes ($\Delta x = 0.0625\ mm$), with refinement at 41, 81, 161, and 321 nodes.

Sensitivity Analysis

Local normalised sensitivity is

$$S_p = \left(\frac{\partial u}{\partial p}\right)\left(\frac{p}{u}\right) \quad (9)$$

Estimated with a centred perturbation $\Delta p = 0.01p$ for δ, Q, β, k_w, and D_v. This is local differential analysis and is not a substitute for global uncertainty quantification [7].

Treatment-Effect Metrics

Treatment effects are reported as descriptive model-comparison metrics rather than clinical response criteria. Define $B(t) = L^{-1}\int_0^L u(x,t)dx$ and $AUC = \int_0^T B(t)dt$. Endpoint centre reduction is $R_c = \frac{100[u_c(T) - u_t(T)]}{u_c(T)}$; endpoint burden reduction is $R_B = \frac{100[B_c(T) - B_t(T)]}{B_c(T)}$; and integrated burden reduction is $R_{AUC} = \frac{100[AUC_c - AUC_t]}{AUC_c}$. The terms "tumor-growth inhibition" and "clinical response" are deliberately avoided.

Structural Comparison with The Predecessor Two-State Model

To isolate the effect of model structure, the predecessor two-state system was solved with the same spatial domain, source, transport coefficients, and treatment parameters. The two-state system replaces w by v in the cytotoxic term and therefore treats extracellular nanoparticle exposure as the direct killing variable. This comparison is not intended as a competing biological model; it is a structural diagnostic of parameter interpretation. See (Table 2) Model Structural Comparison.

Table 2. Model Structural Comparison

Model	Centre u at day 5	Normalised β sensitivity
Two-state predecessor	0.673850	+0.128
Three-state revised	0.718891	-0.177

Results

At baseline, the treatment simulation reduces centre tumor density from 0.800 to 0.719 by day 5. The extracellular nanoparticle concentration at the centre reaches 0.311, while the effective intracellular exposure reaches 0.354. The untreated control reaches 0.936 at the same location and time. The endpoint centre reduction is 23.18%. The spatially averaged tumor burden is 0.176 with treatment and 0.202 in the control, corresponding to a 12.70% reduction. The integrated burden is 0.704 versus 0.745, corresponding to a 5.56% reduction over five days. See the Figures: Figure 1. Initial tumor profile and day-5 spatial distributions of tumor density, extracellular nanoparticles, and effective intracellular exposure (Figure 2); tumor-centre dynamics in the localised-treatment simulation and matched untreated control, and Figure 3. Spatially averaged tumor burden over the five-day simulation.

Spatial Refinement and Numerical Checks

Note (Table 3) Mesh refinement convergence, Figure 4. Centre tumor density at day 5 under spatial mesh refinement. The 161-to-321-node change is approximately 0.023%. The observed refinement orders over the final two intervals are close to two, consistent with the second-order interior discretisation.

Table 3. Mesh refinement convergence.

N_x	$\Delta x\ (mm)$	Centre u at day 5	Change vs previous	Observed order
41	0.25000	0.715260	-	-
81	0.12500	0.718212	0.413%	-
161	0.06250	0.718891	0.094%	2.12
321	0.03125	0.719057	0.023%	2.03

Local Sensitivity

Observe (Table 4) Local normalised sensitivities around the baseline set, and Figure 5. Local normalised sensitivities around the baseline parameter set, for a clear indication of the change in the result.

Copyright *Author (s) 2026. Distributed under Creative Commons CC BY 4.0*
Received: *26-08-2026 -* ***Accepted:*** *24-10-2026 -* ***Published:*** *01-11-2026*

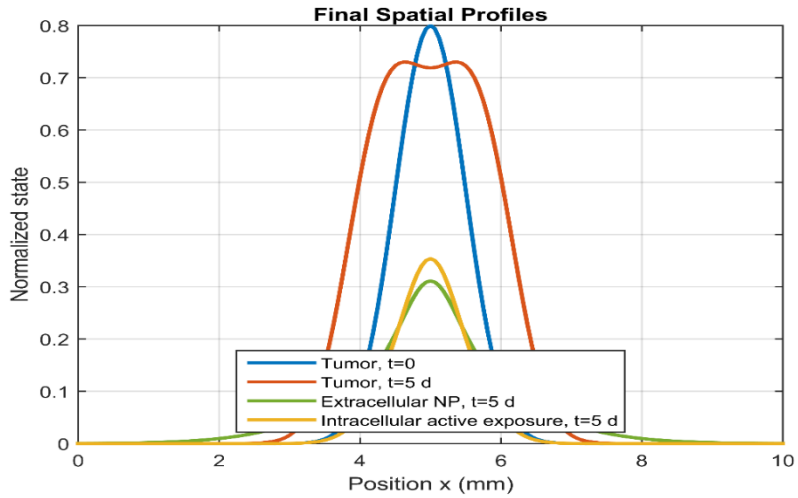


Figure 1. Initial tumor profile and day-5 spatial distributions of tumor density, extracellular nanoparticles, and effective intracellular exposure.

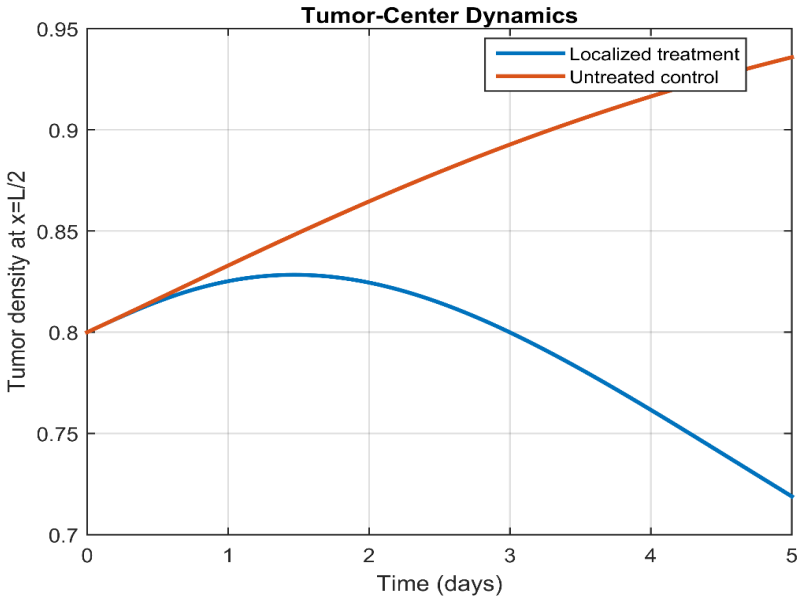


Figure 2. Tumor-center dynamics in the localised-treatment simulation and matched untreated control.

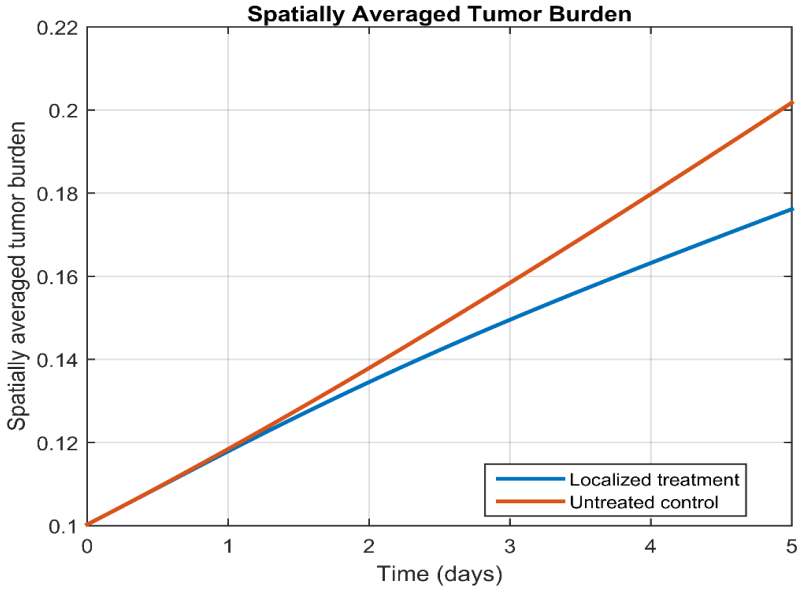


Figure 3. Spatially averaged tumor burden over the five-day simulation.

Copyright *Author (s) 2026. Distributed under Creative Commons CC BY 4.0*
Received: *26-08-2026 -* ***Accepted:*** *24-10-2026 -* ***Published:*** *01-11-2026*

https://doi.org/10.54361/ajmas.261101

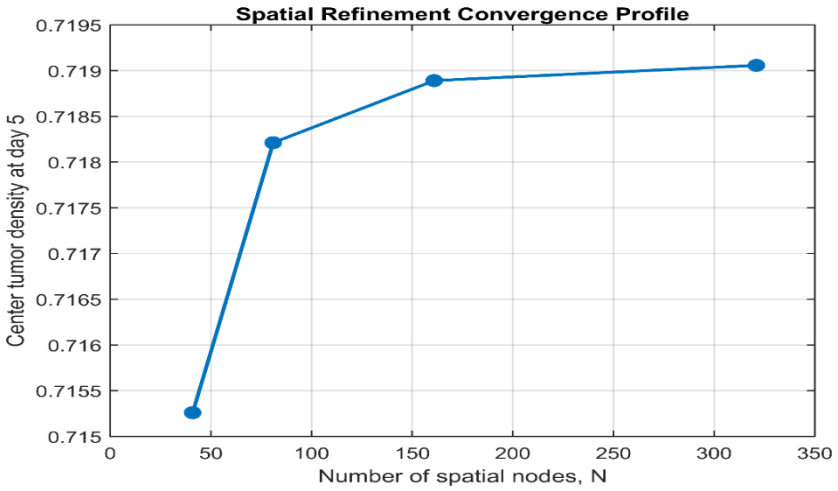


Figure 4. Centre tumor density at day 5 under spatial mesh refinement.

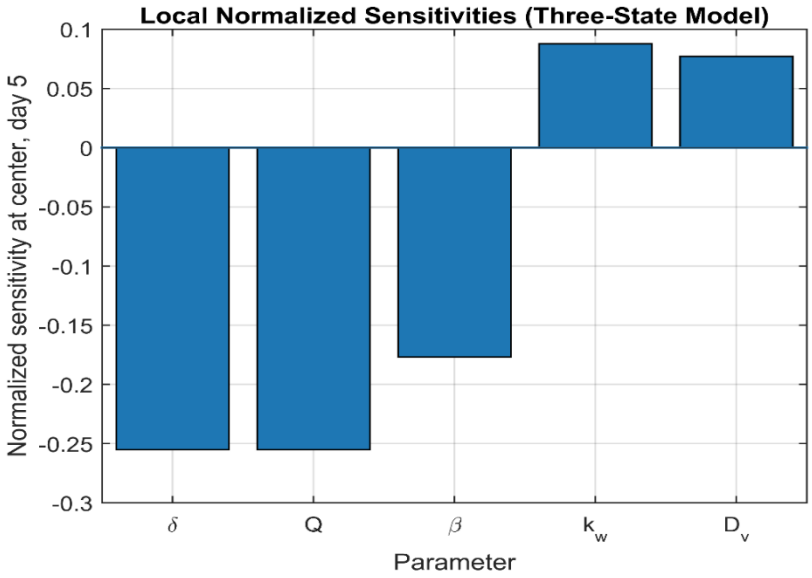


Figure 5. Local normalised sensitivities around the baseline parameter set.

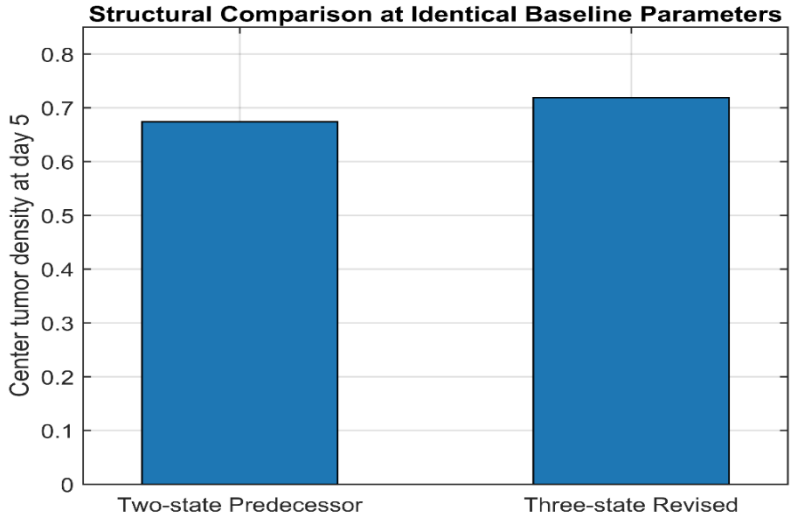


Figure 6. Structural comparison of the predecessor two-state and revised three-state formulations at identical baseline transport parameters.

Copyright *Author (s) 2026. Distributed under Creative Commons CC BY 4.0*
Received: *26-08-2026 -* ***Accepted:*** *24-10-2026 -* ***Published:*** *01-11-2026*

https://doi.org/10.54361/ajmas.261101

Table 4. Local normalised sensitivities around the baseline set

Parameter	Normalised sensitivity at centre, day 5	Interpretation
δ	-0.255	Increasing δ lowers tumor density
Q	-0.255	Increasing source lowers tumor density
β	-0.177	Increasing uptake increases effective intracellular exposure
k_w	0.088	Faster intracellular loss weakens exposure.
D_v	0.077	Faster spreading has a weak positive local sensitivity.

Structural Interpretation Of β

In the predecessor two-state model, the day-5 centre value is 0.674, and the local normalised β sensitivity is +0.128. In the revised three-state model, the corresponding values are 0.719 and -0.177. The sign reversal is the central structural result: uptake is not inherently beneficial or harmful; its effect depends on whether uptake feeds an active intracellular state or merely removes extracellular material. See Figure 6. Structural comparison of the predecessor two-state and revised three-state formulations at identical baseline transport parameters.

Discussion

The revised model produces a modest but reproducible treatment effect under the illustrative baseline parameters. The centre density decreases from 0.800 to 0.719, while the matched untreated control increases to 0.936. The spatially averaged burden is 0.176 under treatment versus 0.202 in the control at day 5, and the integrated burden is 0.704 versus 0.745. The effect is therefore incomplete and should be interpreted as a property of the specified parameter scenario, not as evidence of therapeutic efficacy in osteosarcoma. The most informative result is structural rather than numerical. In the predecessor two-state model, increasing β removes extracellular nanoparticles and therefore can increase tumor density. At the same baseline transport parameters, the two-state model gives a day-5 centre density of 0.674 and a positive normalised β sensitivity of +0.128. This counter-intuitive behaviour stems entirely from a structural anomaly: uptake was modelled as a simple sinking term for the extracellular state without being coupled explicitly to a dedicated intracellular killing field.

Consequently, higher uptake simply depleted the extracellular therapeutic agent prematurely. After adding the effective intracellular exposure state, the same parameter perturbation gives a centre density of 0.719 and a negative β sensitivity of -0.177. The sign reversal is a direct consequence of how uptake is represented in the equations, illustrating how the intermediate field w acts as a mechanistic bridge translating extracellular clearance into direct intracellular cell death via $-\delta uw$. This demonstrates why the biological interpretation of an uptake parameter should not be inferred from its label alone. The baseline sensitivity analysis ranks δ and Q as the strongest inhibitory parameters, followed by β, while k_w and D_v have positive local sensitivities at the centre. These are local differential sensitivities around one illustrative parameter set. They should not be interpreted as global importance rankings because credible parameter distributions and experimental ranges are not available [7]. The numerical test supports the computational implementation. The 161-node solution changes by only about 0.023% when the grid is refined to 321 nodes, and the observed refinement rates are approximately second order. The source normalisation keeps total input Q invariant across meshes. The corrected Robin signs produce symmetric outward leakage. The code also reports minimum state values and uses a nonnegativity safeguard, but that safeguard is not presented as a mathematical proof of positivity.

Several limitations remain. The geometry is one-dimensional and homogeneous, whereas real osteosarcoma tissue is spatially heterogeneous. The source represents localised delivery rather than a full systemic pharmacokinetic process. The effective intracellular state compresses uptake, intracellular processing, and release into one reduced-order variable. No experimental data were used for calibration or external validation, and no global uncertainty or formal identifiability analysis was attempted [5,6]. These limitations are deliberate boundaries of the present study, not claims of clinical readiness. Future work should add data only when those data support the added parameters: spatial nanoparticle penetration measurements, time-resolved intracellular payload measurements, tumor-density imaging, and independent validation data. An image-derived two- or three-dimensional geometry would be a natural extension after calibration. The objective should be to improve identifiability and biological testability rather than to increase model complexity for its own sake [5].

Conclusions

We developed a reduced-order three-state reaction-diffusion model that links localised extracellular nanoparticle transport to effective intracellular active-payload exposure and tumor response. The improved formulation removes the ambiguity of treating uptake and cytotoxic action through the same extracellular variable, while retaining a deliberately small number of states. At the illustrative baseline, the model predicts a 23.18% lower centre tumor density, a 12.70% lower spatially averaged burden at day 5, and a 5.56% lower integrated burden over five days relative to the matched untreated control. The model does not predict tumor eradication, clinical benefit, or patient-specific response. The key methodological result is that the sign and interpretation of uptake sensitivity depend on model structure: β becomes inhibitory only when uptake feeds an intracellular active-exposure state. The framework is therefore most appropriately

Copyright *Author (s) 2026. Distributed under Creative Commons CC BY 4.0*
Received: *26-08-2026 -* ***Accepted:*** *24-10-2026 -* ***Published:*** *01-11-2026*

viewed as a reproducible computational benchmark and hypothesis-generation model. Experimental calibration, parameter identifiability, and independent validation are required before translational use.

Reproducibility and Declarations

Code Availability

The MATLAB code is in Appendix A (MATLAB release: R2015a).

Data Availability

No patient, animal, or experimental dataset was used. All baseline numerical outputs are generated from the equations and parameters reported.

Study Status

This is a computational mechanistic modelling study. It is not clinically validated and must not be used for treatment decisions.

Funding

This research received no external funding.

References

1. Le T, Su S, Kirshtein A, Shahriyari L. Data-driven mathematical model of osteosarcoma. Cancers (Basel). 2021;13(10):2367.
2. Chen C, Wang S, Wang J, Yao F, Tang X, Guo W. Nanosized drug delivery strategies in osteosarcoma chemotherapy. APL Bioeng. 2023;7(1):011501.
3. Dogra P, Butner JD, Chuang YL, Caserta S, Goel S, Brinker CJ, Cristini V, Wang Z. Mathematical modeling in cancer nanomedicine: a review. Biomed Microdevices. 2019;21:40.
4. Stillman NR, Kovacevic M, Balaz I, Hauert S. In silico modelling of cancer nanomedicine, across scales and transport barriers. NPJ Comput Mater. 2020;6:92.
5. Moradi Kashkooli F, Soltani M, Momeni MM, Rahmim A. Enhanced drug delivery to solid tumors via drug-loaded nanocarriers: an image-based computational framework. Front Oncol. 2021;11:655781.
6. Kazerouni AS, Gadde M, Gardner A, Hormuth DA 2nd, Jarrett AM, Johnson KE, et al. Integrating quantitative assays with biologically based mathematical modeling for predictive oncology. iScience. 2020;23(12):101807.
7. Mester R, Landeros A, Rackauckas C, Lange K. Differential methods for assessing sensitivity in biological models. PLoS Comput Biol. 2022;18(6):e1009598.
8. Sun D, Zhou S, Gao W. What went wrong with anticancer nanomedicine design and how to make it right. ACS Nano. 2020;14(10):12281-12290.

Appendix A

The MATLAB Codes

MATLAB Code (1). Results, Figure 1, Figure 2, and Figure 3.

```
function main_simulation
  clc
  clear
  close all
  p.L    = 10.0;        % (mm)
  p.Du   = 0.01;        % (mm^2/day)
  p.Dv   = 0.25;        % (mm^2/day)
  p.r    = 0.40;        % (day^-1)
  p.K    = 1.00;
  p.delta = 0.50;       % (day^-1)
  p.lambda= 0.10;       % (day^-1)
  p.beta  = 0.60;       % (day^-1)
  p.kw   = 0.25;        % (day^-1)
  p.gamma_u = 0.05;     % (mm/day)
  p.gamma_v = 0.12;     % (mm/day)
  p.Q    = 0.30;        % (mm/day)
  p.sigma_q = 0.25;     % (mm)
  p.sigma_u0 = 0.50;    % (mm)
  p.T    = 5.0;         % (days)
  p.Nx   = 161;
  x = linspace(0, p.L, p.Nx)';
  dx = p.L / (p.Nx - 1);
  tspan = linspace(0, p.T, 100);
```

Copyright *Author (s) 2026. Distributed under Creative Commons CC BY 4.0*
Received: *26-08-2026 -* ***Accepted:*** *24-10-2026 -* ***Published:*** *01-11-2026*

https://doi.org/10.54361/ajmas.261101

```
g_x = exp( -((x - p.L/2).^2) / (2 * p.sigma_q^2) );
integral_g = trapz(x, g_x);
q_x = (p.Q * g_x) / integral_g;
u0 = 0.8 * exp( -((x - p.L/2).^2) / (2 * p.sigma_u0^2) );
v0 = zeros(p.Nx, 1);
w0 = zeros(p.Nx, 1);
Y0_treatment = [u0; v0; w0];
Y0_control = [u0; zeros(p.Nx, 1); zeros(p.Nx, 1)];
options = odeset('RelTol', 1e-7, 'AbsTol', 1e-9);
[t, Y_treat] = ode15s(@(t, Y) rhs_pde(t, Y, p, dx, q_x, true), tspan, Y0_treatment, options);
  [~, Y_ctrl]  = ode15s(@(t, Y) rhs_pde(t, Y, p, dx, q_x, false), tspan, Y0_control, options);
Nx = p.Nx;
u_t = Y_treat(:, 1:Nx);
v_t = Y_treat(:, Nx+1:2*Nx);
w_t = Y_treat(:, 2*Nx+1:3*Nx);
u_c = Y_ctrl(:, 1:Nx);
center_idx = round((Nx + 1) / 2);
u_center_treat_end = u_t(end, center_idx);
u_center_control_end = u_c(end, center_idx);
Rc = 100 * (u_center_control_end - u_center_treat_end) / u_center_control_end;
B_treat_end = trapz(x, u_t(end, :)) / p.L;
B_control_end = trapz(x, u_c(end, :)) / p.L;
RB = 100 * (B_control_end - B_treat_end) / B_control_end;
B_treat_all = zeros(length(t), 1);
B_control_all = zeros(length(t), 1);
for i = 1:length(t)
  B_treat_all(i) = trapz(x, u_t(i, :)) / p.L;
  B_control_all(i) = trapz(x, u_c(i, :)) / p.L;
end
AUC_treat = trapz(t, B_treat_all);
AUC_control = trapz(t, B_control_all);
RAUC = 100 * (AUC_control - AUC_treat) / AUC_control;
fprintf('=== RESULTS VERIFICATION ===\n');
fprintf('Initial Center Tumor Density       : %.4f (Expected: 0.8000)\n', u_t(1, center_idx));
fprintf('Final Center Tumor Density (Treat)  : %.4f (Expected: 0.7189)\n', u_center_treat_end);
fprintf('Final Center Tumor Density (Control): %.4f (Expected: 0.9360)\n', u_center_control_end);
fprintf('Endpoint Center Reduction (Rc)      : %.2f%%\n', Rc);
fprintf('Endpoint Burden Reduction (RB)      : %.2f%%\n', RB);
fprintf('Integrated Burden Reduction (RAUC)  : %.2f%%\n', RAUC);
fprintf('============================\n');
figure('Name', 'Final Spatial Profiles', 'Color', 'w');
plot(x, u_t(1, :), 'LineWidth', 2, 'Color', [0 0.4470 0.7410]); hold on;
plot(x, u_t(end, :), 'LineWidth', 2, 'Color', [0.8500 0.3250 0.0980]);
plot(x, v_t(end, :), 'LineWidth', 2, 'Color', [0.4660 0.6740 0.1880]);
plot(x, w_t(end, :), 'LineWidth', 2, 'Color', [0.9290 0.6940 0.1250]);
xlabel('Position x (mm)');
ylabel('Normalized state');
title('Final Spatial Profiles');
legend('Tumor, t=0', 'Tumor, t=5 d', 'Extracellular NP, t=5 d', 'Intracellular active exposure, t=5 d',
'Location', 'best');
grid on;
figure('Name', 'Tumor-Center Dynamics', 'Color', 'w');
plot(t, u_t(:, center_idx), 'LineWidth', 2, 'Color', [0 0.4470 0.7410]); hold on;
plot(t, u_c(:, center_idx), 'LineWidth', 2, 'Color', [0.8500 0.3250 0.0980]);
xlabel('Time (days)');
ylabel('Tumor density at x=L/2');
title('Tumor-Center Dynamics');
legend('Localized treatment', 'Untreated control', 'Location', 'best');
grid on;
figure('Name', 'Spatially Averaged Tumor Burden', 'Color', 'w');
plot(t, B_treat_all, 'LineWidth', 2, 'Color', [0 0.4470 0.7410]); hold on;
```

Copyright *Author (s) 2026. Distributed under Creative Commons CC BY 4.0*
Received*: 26-08-2026 -* ***Accepted****: 24-10-2026 -* ***Published****: 01-11-2026*

https://doi.org/10.54361/ajmas.261101

```
  plot(t, B_control_all, 'LineWidth', 2, 'Color', [0.8500 0.3250 0.0980]);
  xlabel('Time (days)');
  ylabel('Spatially averaged tumor burden');
  title('Spatially Averaged Tumor Burden');
  legend('Localized treatment', 'Untreated control', 'Location', 'best');
  grid on;
end
function dYdt = rhs_pde(~, Y, p, dx, q_x, is_treated)
  Nx = p.Nx;
  u = Y(1:Nx);
  v = Y(Nx+1:2*Nx);
  w = Y(2*Nx+1:3*Nx);
  uxx = zeros(Nx, 1);
  vxx = zeros(Nx, 1);
  for i = 2:(Nx-1)
    uxx(i) = (u(i+1) - 2*u(i) + u(i-1)) / dx^2;
    vxx(i) = (v(i+1) - 2*v(i) + v(i-1)) / dx^2;
  end
  uxx(1) = 2 * (u(2) - u(1) - (p.gamma_u * dx / p.Du) * u(1)) / dx^2;
  vxx(1) = 2 * (v(2) - v(1) - (p.gamma_v * dx / p.Dv) * v(1)) / dx^2;

  uxx(Nx) = 2 * (u(Nx-1) - u(Nx) - (p.gamma_u * dx / p.Du) * u(Nx)) / dx^2;
  vxx(Nx) = 2 * (v(Nx-1) - v(Nx) - (p.gamma_v * dx / p.Dv) * v(Nx)) / dx^2;
  dudt = p.Du * uxx + p.r * u .* (1.0 - u / p.K) - p.delta * u .* w;
  if is_treated
    dvdt = p.Dv * vxx - p.lambda * v - p.beta * u .* v + q_x;
  else
    dvdt = zeros(Nx, 1);
  end
  if is_treated
    dwdt = p.beta * u .* v - p.kw * w;
  else
    dwdt = zeros(Nx, 1);
  end
  dYdt = [dudt; dvdt; dwdt];
end
```

MATLAB Code (2). Results and Figure 4.

```
function mesh_refinement_tests
clc
clear
close all
  p.L    = 10.0;
  p.Du   = 0.01;
  p.Dv   = 0.25;
  p.r    = 0.40;
  p.K    = 1.00;
  p.delta = 0.50;
  p.lambda= 0.10;
  p.beta  = 0.60;
  p.kw   = 0.25;
  p.gamma_u = 0.05;
  p.gamma_v = 0.12;
  p.Q    = 0.30;
  p.sigma_q = 0.25;
  p.sigma_u0 = 0.50;
  p.T    = 5.0;
  Nx_list = horzcat(41, 81, 161, 321);
  u_center_results = zeros(size(Nx_list));
  dx_list = zeros(size(Nx_list));
  options = odeset('RelTol', 1e-8, 'AbsTol', 1e-10);
```

Copyright *Author (s) 2026. Distributed under Creative Commons CC BY 4.0*
Received: *26-08-2026 -* ***Accepted:*** *24-10-2026 -* ***Published:*** *01-11-2026*

https://doi.org/10.54361/ajmas.261101

```
    fprintf('=== RUNNING MESH REFINEMENT CONVERGENCE ===\n');
    fprintf('%-6s\t%-10s\t%-20s\t%-15s\n', 'Nx', 'dx (mm)', 'Center u at Day 5', 'Change vs Prev');
    for k = 1:length(Nx_list)
        Nx = Nx_list(k);
        p_current = p;
        p_current.Nx = Nx;
        dx = p.L / (Nx - 1);
        dx_list(k) = dx;
        u_center_results(k) = solve_specific_mesh(p_current, options);
        if k == 1
            fprintf('%-6d\t%-10.5f\t%-20.6f\t%-15s\n', Nx, dx, u_center_results(k), '-');
        else
            pct_change = 100 * abs(u_center_results(k) - u_center_results(k-1)) / u_center_results(k-1);
            fprintf('%-6d\t%-10.5f\t%-20.6f\t%.3f%%\n', Nx, dx, u_center_results(k), pct_change);
        end
    end
    fprintf('\n=== CALCULATED OBSERVED ORDER ===\n');
    for k = 3:length(Nx_list)
        diff_prev = abs(u_center_results(k-1) - u_center_results(k-2));
        diff_curr = abs(u_center_results(k) - u_center_results(k-1));
        observed_order = log(diff_prev / diff_curr) / log(2);
        fprintf('Interval (Nx = %d -> %d -> %d): Observed Order = %.2f\n', ...
            Nx_list(k-2), Nx_list(k-1), Nx_list(k), observed_order);
    end
fprintf('====================================\n');
    figure('Name', 'Spatial Refinement Convergence', 'Color', 'w');
    plot(Nx_list, u_center_results, '-o', 'LineWidth', 1.8, 'MarkerSize', 7, ...
        'MarkerFaceColor', [0 0.4470 0.7410], 'Color', [0 0.4470 0.7410]);
    xlabel('Number of spatial nodes, N');
    ylabel('Center tumor density at day 5');
    title('Spatial Refinement Convergence Profile');
    grid on;
end
function u_center = solve_specific_mesh(p, options)
    Nx = p.Nx;
    x = linspace(0, p.L, Nx)';
    dx = p.L / (Nx - 1);
    tspan = [0, p.T];
    g_x = exp( -((x - p.L/2).^2) / (2 * p.sigma_q^2) );
    q_x = (p.Q * g_x) / trapz(x, g_x);
    u0 = 0.8 * exp( -((x - p.L/2).^2) / (2 * p.sigma_u0^2) );
    Y0 = [u0; zeros(Nx, 1); zeros(Nx, 1)];
    [~, Y] = ode15s(@(t, Y) rhs_core(t, Y, p, dx, q_x), tspan, Y0, options);
    center_idx = round((Nx + 1) / 2);
    u_final = Y(end, 1:Nx);
    u_center = u_final(center_idx);
end
function dYdt = rhs_core(~, Y, p, dx, q_x)
    Nx = p.Nx;
    u = Y(1:Nx); v = Y(Nx+1:2*Nx); w = Y(2*Nx+1:3*Nx);
    uxx = zeros(Nx, 1); vxx = zeros(Nx, 1);
    for i = 2:(Nx-1)
        uxx(i) = (u(i+1) - 2*u(i) + u(i-1)) / dx^2;
        vxx(i) = (v(i+1) - 2*v(i) + v(i-1)) / dx^2;
    end
    uxx(1) = 2 * (u(2) - u(1) - (p.gamma_u * dx / p.Du) * u(1)) / dx^2;
    vxx(1) = 2 * (v(2) - v(1) - (p.gamma_v * dx / p.Dv) * v(1)) / dx^2;
    uxx(Nx) = 2 * (u(Nx-1) - u(Nx) - (p.gamma_u * dx / p.Du) * u(Nx)) / dx^2;
    vxx(Nx) = 2 * (v(Nx-1) - v(Nx) - (p.gamma_v * dx / p.Dv) * v(Nx)) / dx^2;
    dudt = p.Du * uxx + p.r * u .* (1.0 - u / p.K) - p.delta * u .* w;
    dvdt = p.Dv * vxx - p.lambda * v - p.beta * u .* v + q_x;
```

Copyright *Author (s) 2026. Distributed under Creative Commons CC BY 4.0*
Received: *26-08-2026 -* ***Accepted:*** *24-10-2026 -* ***Published:*** *01-11-2026*

https://doi.org/10.54361/ajmas.261101

```
  dwdt = p.beta * u .* v - p.kw * w;
  dYdt = [dudt; dvdt; dwdt];
end
```

MATLAB Code (3). Results, Figure 5, and Figure 6.

```
function sensitivity_and_comparison
clc
clear
close all
  p.L    = 10.0;
  p.Du   = 0.01;
  p.Dv   = 0.25;
  p.r    = 0.40;
  p.K    = 1.00;
  p.delta = 0.50;
  p.lambda= 0.10;
  p.beta  = 0.60;
  p.kw   = 0.25;
  p.gamma_u = 0.05;
  p.gamma_v = 0.12;
  p.Q    = 0.30;
  p.sigma_q = 0.25;
  p.sigma_u0 = 0.50;
  p.T    = 5.0;
  p.Nx   = 161;
  options = odeset('RelTol', 1e-7, 'AbsTol', 1e-9);
  fprintf('=== RUNNING STRUCTURAL COMPARISON ===\n');
  u_three = solve_model(p, options, 3);
  u_two = solve_model(p, options, 2);
  fprintf('Two-state predecessor model center u: %.6f (Expected: 0.673850)\n', u_two);
  fprintf('Three-state revised model center u   : %.6f (Expected: 0.718891)\n', u_three);
fprintf('=====================================\n\n');
  fprintf('=== CALCULATING LOCAL SENSITIVITIES ===\n');
  target_params = {'delta', 'Q', 'beta', 'kw', 'Dv'};
  S_three = zeros(1, length(target_params));
  for i = 1:length(target_params)
    param_name = target_params{i};
    p_base = p.(param_name);
    dp = 0.01 * p_base;
    p_plus = p; p_plus.(param_name) = p_base + dp;
    u_plus = solve_model(p_plus, options, 3);
    p_minus = p; p_minus.(param_name) = p_base - dp;
    u_minus = solve_model(p_minus, options, 3);
    dudp = (u_plus - u_minus) / (2 * dp);
    S_three(i) = dudp * (p_base / u_three);
    fprintf('Sensitivity of %-5s: %+.3f\n', param_name, S_three(i));
  end
  dp_beta = 0.01 * p.beta;
  p_plus = p; p_plus.beta = p.beta + dp_beta;
  u_plus_two = solve_model(p_plus, options, 2);
  p_minus = p; p_minus.beta = p.beta - dp_beta;
  u_minus_two = solve_model(p_minus, options, 2);
  dudp_two = (u_plus_two - u_minus_two) / (2 * dp_beta);
  S_two_beta = dudp_two * (p.beta / u_two);
  fprintf('Sensitivity of beta (Two-state): %+.3f (Expected: +0.128)\n', S_two_beta);
fprintf('=====================================\n');
  figure('Name', 'Local Normalized Sensitivity', 'Color', 'w');
  hBar = bar(S_three, 'FaceColor', [0.1176 0.4667 0.7059]);
  set(gca, 'XTickLabel', {'\delta', 'Q', '\beta', 'k_w', 'D_v'}, 'FontSize', 11);
  xlabel('Parameter');
  ylabel('Normalized sensitivity at center, day 5');
  title('Local Normalized Sensitivities (Three-State Model)');
```

Copyright *Author (s) 2026. Distributed under Creative Commons CC BY 4.0*
Received*: 26-08-2026 -* ***Accepted****: 24-10-2026 -* ***Published****: 01-11-2026*

https://doi.org/10.54361/ajmas.261101

```
    grid on; hold on;
    line([0, 6], [0, 0], 'Color', [0.1176 0.4667 0.7059], 'LineWidth', 0.8); xlim([0.5, 5.5]);
    figure('Name', 'Structural Comparison', 'Color', 'w');
    bar_data = [u_two, u_three];
    bar(bar_data, 0.5, 'FaceColor', [0.1176 0.4667 0.7059]);
    set(gca, 'XTickLabel', {'Two-state Predecessor', 'Three-state Revised'}, 'FontSize', 11);
    ylabel('Center tumor density at day 5');
    title('Structural Comparison at Identical Baseline Parameters');
    grid on;
    ylim([0, 0.85]);
end
function u_center = solve_model(p, options, model_type)
    Nx = p.Nx;
    x = linspace(0, p.L, Nx)';
    dx = p.L / (Nx - 1);
    tspan = [0, p.T];
    g_x = exp( -((x - p.L/2).^2) / (2 * p.sigma_q^2) );
    q_x = (p.Q * g_x) / trapz(x, g_x);
    u0 = 0.8 * exp( -((x - p.L/2).^2) / (2 * p.sigma_u0^2) );
    if model_type == 3
        Y0 = [u0; zeros(Nx, 1); zeros(Nx, 1)];
        [~, Y] = ode15s(@(t, Y) rhs_three_state(t, Y, p, dx, q_x), tspan, Y0, options);
        u_final = Y(end, 1:Nx)';
    else
        Y0 = [u0; zeros(Nx, 1)];
        [~, Y] = ode15s(@(t, Y) rhs_two_state(t, Y, p, dx, q_x), tspan, Y0, options);
        u_final = Y(end, 1:Nx)';
    end
    center_idx = round((Nx + 1) / 2);
    u_center = u_final(center_idx);
end
function dYdt = rhs_three_state(~, Y, p, dx, q_x)
    Nx = p.Nx;
    u = Y(1:Nx); v = Y(Nx+1:2*Nx); w = Y(2*Nx+1:3*Nx);
    uxx = zeros(Nx, 1); vxx = zeros(Nx, 1);
    for i = 2:(Nx-1)
        uxx(i) = (u(i+1) - 2*u(i) + u(i-1)) / dx^2;
        vxx(i) = (v(i+1) - 2*v(i) + v(i-1)) / dx^2;
    end
    uxx(1) = 2 * (u(2) - u(1) - (p.gamma_u * dx / p.Du) * u(1)) / dx^2;
    vxx(1) = 2 * (v(2) - v(1) - (p.gamma_v * dx / p.Dv) * v(1)) / dx^2;
    uxx(Nx) = 2 * (u(Nx-1) - u(Nx) - (p.gamma_u * dx / p.Du) * u(Nx)) / dx^2;
    vxx(Nx) = 2 * (v(Nx-1) - v(Nx) - (p.gamma_v * dx / p.Dv) * v(Nx)) / dx^2;
    dudt = p.Du * uxx + p.r * u .* (1.0 - u / p.K) - p.delta * u .* w;
    dvdt = p.Dv * vxx - p.lambda * v - p.beta * u .* v + q_x;
    dwdt = p.beta * u .* v - p.kw * w;
    dYdt = [dudt; dvdt; dwdt];
end
function dYdt = rhs_two_state(~, Y, p, dx, q_x)
    Nx = p.Nx;
    u = Y(1:Nx); v = Y(Nx+1:2*Nx);
    uxx = zeros(Nx, 1); vxx = zeros(Nx, 1);
    for i = 2:(Nx-1)
        uxx(i) = (u(i+1) - 2*u(i) + u(i-1)) / dx^2;
        vxx(i) = (v(i+1) - 2*v(i) + v(i-1)) / dx^2;
    end
    uxx(1) = 2 * (u(2) - u(1) - (p.gamma_u * dx / p.Du) * u(1)) / dx^2;
    vxx(1) = 2 * (v(2) - v(1) - (p.gamma_v * dx / p.Dv) * v(1)) / dx^2;
    uxx(Nx) = 2 * (u(Nx-1) - u(Nx) - (p.gamma_u * dx / p.Du) * u(Nx)) / dx^2;
    vxx(Nx) = 2 * (v(Nx-1) - v(Nx) - (p.gamma_v * dx / p.Dv) * v(Nx)) / dx^2;
    dudt = p.Du * uxx + p.r * u .* (1.0 - u / p.K) - p.delta * u .* v;
```

Copyright *Author (s) 2026. Distributed under Creative Commons CC BY 4.0*
Received: *26-08-2026 -* ***Accepted:*** *24-10-2026 -* ***Published:*** *01-11-2026*

https://doi.org/10.54361/ajmas.261101

```
    dvdt = p.Dv * vxx - p.lambda * v - p.beta * u .* v + q_x;
    dYdt = [dudt; dvdt];
end
```

Copyright *Author (s) 2026. Distributed under Creative Commons CC BY 4.0*
Received*: 26-08-2026 -* ***Accepted****: 24-10-2026 -* ***Published****: 01-11-2026*